



Numerical Investigation of Transient Heat Transfer Process in Organic Phase Change Material (OPCM) - Airheat Exchanger

Abiodun A. IDRIS^{1*}, Kafayat ADEYEMI¹, Nasir LAWAL¹

¹Department of Mechanical Engineering, University of Abuja, Nigeria

* Corresponding author: abiodumidris@yahoo.com

Abstract

This paper presents the analysis of the numerical investigation of the Transient cooling heat transfer process of air flow within a circular duct, embedded in a rectangular container of PureTemp20- a bio-based Organic Phase Change Material (OPCM) with applications in Heating Ventilation and Air Conditioning. The heat transfer process was studied by constructing an axisymmetric 2-D geometrical model of the domain in GAMBIT 2.4.6, while the numerical simulation of the melting process was done using ANSYS FLUENT 6.3 enthalpy-porosity approach. The simulation shows heat transfer pattern from ambient Air to OPCM as well as thermal and hydro dynamic boundary development within the duct. Also, the cross-sectional velocity profile and static temperature within the duct were simulated. During the first stage of the OPCM melting process heat conduction was the main heat transfer mechanism, but as melting progresses heat transfer takes the form of natural convection. This slows down heat transfer rate from Air to OPCM. This indicates that the heat transfer from Air to OPCM starts at the OPCM's solidus temperature with conduction controlled heat transfer process (CDC-HTP), and as the OPCM starts to melt Free Convection controlled heat transfer process (FCC-HTP) set in, while the effect of CDC-HTP is minimal. Simulations of Instantaneous air flow velocity $u(r)$ distributions and Instantaneous Static Temperature $T(r)$ profiles agreed with published research works within the hydro-dynamically and thermally developing region. Thermal boundary layer is thicker than the Velocity boundary layer in the Air Duct. Thus, Prandtl number (Pr) of Air is less than 1. This confirms Prandtl number $Pr=0.7 < 1$ in published research works.

Keywords

Transient Numerical Simulation; PureTemp20; Latent Energy Storage; Heat Exchanger; Liquefaction.

1.0 Introduction

There are several studies on different PCM – Air heat exchanger configurations for heat transfer process in the Heating, Ventilation and air Conditioning (HVAC) system applications. Some of these configurations are: a cellular structure where cubic PCM and air channels were alternated (Herbinger et al., 2016); parallel PCMs slabs with rectangular air flow channels

in-between (Chen D. et al. 2020; Vakialtojjar et al., 2001); cross-flow heat exchangers where one (Dubovsky et al., 2011) or multiple PCMs (Ezra et al., 2016) filled tubes and air is driven across the tubes bank. Heat exchanger geometries with PCM slabs and air gaps are the most studied of all for thermal energy storage in building ventilation systems. They have been the subject of intensive experimental development where real-scale prototypes have been built and tested (Dolado et al., 2011; Gowreesunker B.L. et al 2013; Labat M. et al., 2014) and the results have been used to validate numerical analysis (Dolado et al., 2011; Gowreesunker et al., 2013) for further optimization of the heat storage system.

In this study, the PCM – Air heat exchanger configuration used is a combination of circular duct embedded in a rectangular container of the PCM (Figure 1a). This is to give a basic understanding of the heat flow pattern within the system in order to proffer a better means of enhancing the heat exchanger.

As the laminar incompressible flow of the hotter ambient space air (air-conditioned return air) at temperature of 297.15 (24°C) runs within the duct, it exchanges heat with the colder OPCM convectively, melting it at the phase change temperature of 293.15 K (20°C). Heat transfer in the studied duct is of two modes; the simple conduction mode which is in radial direction, and the heat transfer due to bulk movement of the fluid axially (Kay et al., 2005, Kay W.M.,2011). Prandtl number Pr_{is} the dimensionless number for assessment of the relative influence of the conductive mode and the viscous effects of the associated flow. Prandtl number for the heat transfer fluid (air) in this study is, $Pr_{air} = 0.7$ (Kay et al., 2005; Kay W.M.,2011); the implication is that the rate of heat diffusion (radially) is greater than the rate of diffusion of viscous effects within the flowing air. This essentially means that the rate at which the effects of the PCM-induced temperature changes at the pipe wall spread into the fluid is greater than the rate of spread of the effects of momentum changes in the flow (Kay W.M., 2011).

The main objective of this study was to assess the thermal and fluid flow parameters at the outlet cross-section of the domain for unfinned air duct. Since temperature is a good parameter for assessing the degree of coldness / hotness of a body, its temporal values at the outlet cross-section were determined. To this end, an axisymmetric 2D geometrical model of the domain was constructed in **GAMBIT 2.4.6 (a commercial grid generator)**, taking into account heat transfer within the PCM media, initially by conduction followed by free convection, and heat transfer within the air domain by forced

convection. The melting process was simulated using the enthalpy-porosity approach (FLUENT manual, 2001 of the commercial finite volume software, FLUENT 6.3; Fallahnezhad N. 2020).

Detailed description of the studied geometry, the mathematical model and the mesh sensitivity study are presented in the following section. Also presented is the behaviour of the organic PCM during the melting process.

2.0 Methodology

2.1 Physical Model

Figure 1a shows the sectional view of the PCM – Air heat exchanger configuration used. This indicates a combination of circular duct embedded in a rectangular container of the PCM. Figure 1b is an axisymmetric sketch of the problem under consideration. It refers to a two-dimensional horizontal duct submerged in a container of *PureTemp20*, which is used to store thermal energy. The duct internal radius, $r = 25$ mm, wall thickness $d = 1.5$ mm and a length of $32D$ (1,600mm); while the effective height between the duct surface and the PCM container is $w = 22$ mm and of the same length (1,600mm). An incompressible laminar flow of a space ambient air through the duct, at an inlet Reynolds number $Re_D = 1,546.9$ and an inlet temperature of 297.15 K (24°C), causes heat to be transferred to the *PureTemp20*, converting it from solid to liquid at the phase change temperature of 293.15 K (20°C). The duct length was made less than the hydrodynamic entry length of $x_{fd,h} = 0.05 Re_D D$ obtained from (Langhar H.,1942; Guo L. et al., 2018) and thermal entry length of $x_{fd,th} = 0.05 Re_D D Pr$ obtained from (Kay W.M., 2011), to ensure developing flow at the outlet. Figures 1c shows the computational grids within the OPCM domain [A] and the HTF(Air) domain [B]. The direction of air flow is also indicated.

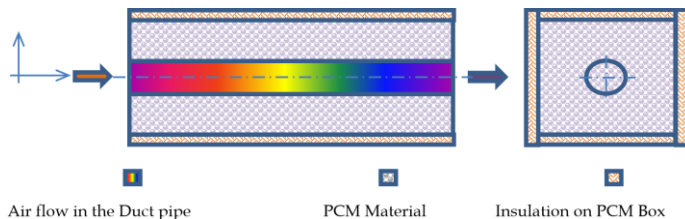


Figure 1a: Schematic of the PCM-Air Heat Exchanger Physical Model

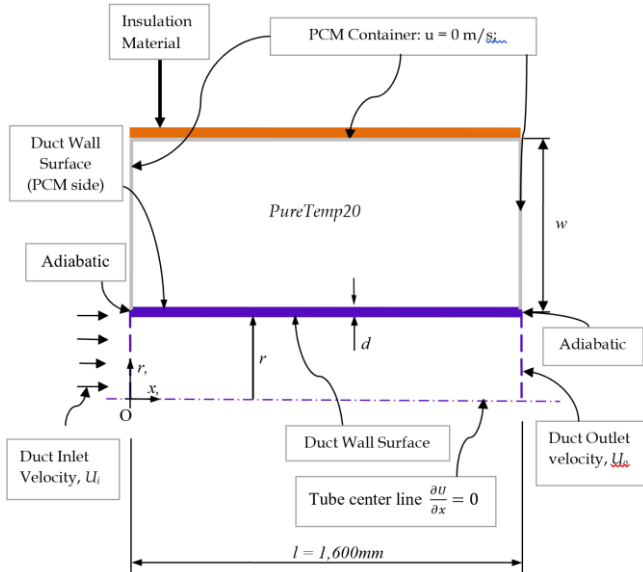


Figure 1b: Axisymmetric sketch of the Computational Domain

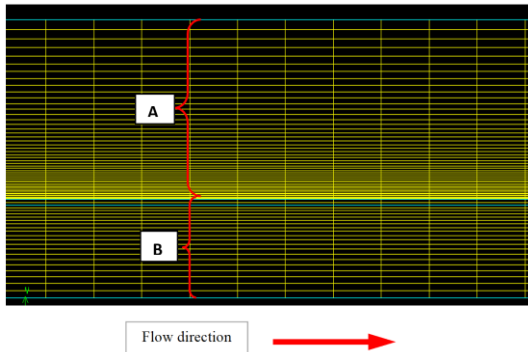


Figure 1c: Computational Grids of OPCM and Air Domains

Table 1: Thermo-physical Properties of PureTemp20 (*PureTemp20 Technical Data sheet, Entropy Solutions*)

S/N	Properties	288.15 K (15°C)	295.15 K (22°C)
1	Density (kg/m ³)	950	860
2	Heat Capacity, C_p (J/kg-K)	2,070	2,150
3	Thermal Conductivity, k (W/m-K)	0.23	0.14
4	Latent Heat of Fusion (J/kg)	171,000	
5	Melting Point, T_{mp}	293.15 K (20°C)	
6	Solidus Temperature, T_{sol}	288.15 K (15°C)	
7	Liquidus Temperature, T_{liq}	295.15 K (22°C)	

Table 2: Thermo-physical Properties of Air (Hosung , 2017, Thermoelectrics: Design &Materials, p.324)

S/N	Properties	293.15K (20°C)	297.15 K (24°C)
1	Density, ρ (kg/m ³)	1.204	1.184
2	Heat Capacity, C_p (J/kg-K)	1007.07	1007.13
3	Thermal Conductivity, k (W/m-K)	0.0264	0.0265
4	Absolute Viscosity, μ (kg/m-s)	1.85e-05	1.86e-05

Table 3: Other Test Conditions

S/N	Parameter	Value
1	Duct diameter, D (m)	0.050
2	Duct Wall Thickness d (m)	0.0015
3	Duct Cross-sectional Area, A (m ²)	0.0019635
4	Inlet Reynolds number (Re_D)	1,546.9
5	Free stream velocity, U_i (m/s)	0.5
6	Inlet Flow rate, Q (m ³ /s)	0.00098175
7	Duct wall material (Aluminum) - thermal conductivity, k	202.4

2.2 Mathematical Model

2.2.1 Assumptions

The assumptions applied to the general transport equation to arrive at the under listed governing equations (1 - 3), for the air domain, and equations (4 - 11), for the PCM domain are:

- i. Unsteady laminar flow of a viscous, incompressible, Newtonian fluid without free-surface effects
- ii. The density, specific heat capacity, thermal conductivity and viscosity of air vary as piecewise linear.
- iii. No heat generation within the air domain.
- iv. Both the solid as well as the liquid phase is homogeneous and isotropic, and the melting process is transient and assumed to be a 2-D phenomenon.
- v. PureTemp20 in the liquid phase is considered to be an incompressible Newtonian fluid.
- vi. Viscous heating and the volume change upon phase change are ignored.
- vii. For the molten PCM, laminar flow as Newtonian fluid is assumed.
- viii. The solid is homogeneously distributed in the mushy region.
- ix. A normal downward-directed gravity field with the corresponding gravitational acceleration of 9.81 m/s² is considered.
- x. The density, specific heat capacity and thermal conductivity of the PCM vary as piecewise linear.
- xi. No heat generation within the PCM.

Continuity Equation

$$\frac{\partial \rho}{\partial t} + \rho(\nabla \cdot \vec{V}) = 0 \quad 1$$

Momentum Equation

$$\rho \frac{\partial \vec{V}}{\partial t} + (\vec{V} \cdot \nabla) \vec{V} = -\frac{1}{\rho} \nabla P + \nu \nabla^2 \vec{V} + S_M \quad 2$$

Energy Equation for Air Domain

$$\frac{\partial T}{\partial t} + (\vec{V} \cdot \nabla) T = \alpha \nabla^2 T + S_E \quad 3$$

Energy Equation for PCM Domain

$$\frac{\partial}{\partial t}(\rho H) + \nabla \cdot (\rho v H) = \nabla \cdot (k \nabla T) + S_E \quad 4$$

with the Total Enthalpy

$$H = H_S + H_{lat} \quad 5$$

and the Sensible Enthalpy

$$H_S = H_{Sref} + \int_{T_{ref}}^T c_p dT \quad 6$$

Latent Heat

The latent heat content can now be written in terms of the latent heat of the material, L as:

$$\Delta H = \beta L$$

To solve the PCM domain, FLUENT 6.3 enthalpy-porosity approach was used. This involves dividing the PCM domain into three regions: liquid, solid and mushy (liquid-solid). The mushy zone is treated as a porous zone with porosity equal to the liquid fraction, which lies between 0 to 1 and generally increases from 0 to 1.

Based on a method proposed by (FLUENT manual, 2001; Herbingier et al., 2016), the liquid fraction, β , can be defined as;

$$\left. \begin{aligned} \beta &= 0 \text{ if } T < T_{sol} \\ \beta &= 1 \text{ if } T > T_{liq} \\ \beta &= \frac{T - T_{sol}}{T_{liq} - T_{sol}} \text{ if } T_{sol} < T < T_{liq} \end{aligned} \right\} \quad 8$$

With $T_{sol} = 288.15$ K (15°C) and $T_{liq} = 295.15$ K (22°C). The size of the mushy zone is determined by the temperatures T_{sol} and T_{liq} . As described in (FLUENT manual, 2001), an iteration between the energy balance Equation (4) and the liquid fraction Equation (8) is done for the calculation of the temperature. This method was suggested by (Voller et al., 1987) because a direct calculation of Equation (8) to update the liquid fractions would result in poor convergence of the energy balance Equation (4). The velocity field within the PCM is obtained from the solution of Equations 9, 10 & 11.

Continuity Equation

$$\frac{\partial \rho}{\partial t} + \nabla \cdot (\rho \vec{V}) = 0 \quad 9$$

Momentum Equation

$$\frac{\partial}{\partial t} (\rho \vec{V}) + \rho \vec{V} \cdot (\nabla \vec{V}) = -\nabla P + \nabla \cdot (2\mu \beta \vec{V}) + A_C (\beta) \vec{V} + \mathcal{S}_M \quad 10$$

with

$$A_C(\beta) = C \frac{(1 - \beta)^2}{\beta^3 + b} \quad 11$$

$A_C(\beta)$ is the porosity function that gradually reduces the velocities from a finite value in the liquid to zero in the solid. To avoid division by zero, the value b , a small computational constant ($b = 0.001$) is introduced in Equation (11). While the mushy zone constant C is supposed to reflect the structure of the melting front. The standard value of the mushy zone constant, $C = 10^5$, in FLUENT 6.3 was used. The higher the value of the mushy zone constant, the steeper the damping term becomes (Hameter et al., 2016)

Mass-Weighted Average velocity at axial locations, $U_x(x)$, within the bulk of the flowing air was calculated by (FLUENT manual, 2001) as:

$$U_x = \frac{\int \rho u(r) u(r) dA}{\int \rho u(r) dA} \quad 12$$

Mass-Weighted Average Static Temperature at axial locations $T_{mx}(x)$ within the bulk of the flowing air was also calculated by (FLUENT manual, 2001) as:

$$T_{mx} = \frac{\int \rho u(r)T(r)dA}{\int \rho u(r)dA} \quad 13$$

Equations (1) - (11) were solved in FLUENT 6.3 to obtain the velocity, temperature and liquid fraction fields within the domain. After an extensive grids independence study, an arrangement of 14,400 cells was found to be sufficient. PRESTO scheme was adopted for pressure interpolation, while the convective terms in the momentum and energy equations were discretized using first order upwind interpolation scheme. Pressure - Velocity coupling was done using SIMPLE algorithm. Convergence was obtained when the residual of the energy, momentum and continuity equations were reduced to less than 10^{-6} , 10^{-3} and 10^{-3} respectively. The time step was set as 0.05s while the number of iterations per time step was set to 20 (Koller et al., 2016). The simulation was performed on 1.86 / 1.87 GHz Intel (R) Pentium (R) Dual CPU T2390 processor with 2 GB RAM.

2.3 Boundary Conditions

In Figure 1b, the boundary conditions and the direction of the gravity used for the numerical simulations are indicated. At the top and the side surfaces of the *PureTemp20* (OPCM) container, as well as the annular ends of the duct wall, an adiabatic wall were defined. The adiabatic boundary conditions prevent heat exchange with the surrounding across these surfaces. Hence, none of the heat transferred to the PCM during the melting process was lost through the adiabatic surfaces. In real thermal heat storage devices, the container was completely insulated against the environment. The thickness of this insulation was chosen in such a way that the thermal loss was as low as economically feasible. Thus, nearly adiabatic conditions were given for such a storage unit. Therefore, the assumption of an adiabatic wall was justified.

Symmetry boundary condition was specified at the centerline of the tube. Upstream of the tube is inlet velocity, where the velocity of the incoming flow was specified as 0.5 m/s. And as energy equations were being solved, the temperature of the incoming airflow was fixed at 297.15 K (24°C). Outflow boundary condition was specified at the outlet to enable outlet airflow properties have zero gradients normal to the outflow face. The inner tube wall

surface temperature was fixed by the flowing air while the upper tube wall surface temperature was fixed by the melting PCM.

3.0 Numerical Results and Discussion

Numerical simulation was carried out on transient cooling of space ambient air, flowing in a thin-walled horizontal circular duct at a Reynolds number of 1,546.9 and an inlet temperature of 297.15 K (24°C). The cooling was provided by melting *PureTemp20* waxy solid (PCM, $T_{mp} = 293.15$ K (20°C)) filled in an adiabatic walled rectangular thermal storage unit enclosing the thin-walled horizontal circular duct longitudinally. At the start of the cooling process, the inlet temperature of ambient air was maintained at a fixed value of 297.15 K (24°C) and the initial temperature of the PCM was 288.15 K (15°C) - the Solidus Temperature. The inlet velocity of the ambient air was maintained at 0.5 m/s. The results are presented and evaluated in this section as follows.

Figure 2 represents contours of temperature distribution with time, near the duct outlet. The blue colour shows the lowest temperature zone while the red colour shows the highest temperature zone. Other colours show temperature zones in between the two. At the initial stage of the cooling process, about 10 minutes into the process, no change in PCM temperature was observed; but the air temperature increases from the wall value (about 294.15 K) to the centerline value of about 297.15 K. Colder air occupies about 40% of the duct cross-section, upper green part containing the thermal and hydrodynamic boundary layers of cold and viscous air.

Moreover, the flow was still developing both thermally and hydrodynamically, as can be seen from the streamline profiles of the contours within the ducts, after about 10 minutes. On the contrary case of the fully developed flow, the red zone, occupying about 60% of the duct cross-section from the centerline, could not be seen towards the outlet of the duct, because the demarcation line of the thermal boundary layer would have merged with the centerline far upstream the outlet.

However, the contour profile is different after 19 minutes into the process, because it relatively has hotter air in the red non-conductive zone. A mixing layer was formed at the interface of the red but faster zone, and the hydrodynamic boundary layer of low-velocity fluid. Transition to turbulence occurs after a very short distance in the flow direction from the point where the

different streams initially meet. The turbulence causes vigorous mixing of adjacent fluid layers that was seen on the contours, since pockets of the hotter and faster air (red zone) entrained in the colder and slower air (green zone).

On the PCM side, after 19 minutes into the process, the temperature starts to rise gradually in the region of the storage container close to the duct wall; this was depicted by the thin lighter blue strip on the upper line of the duct wall. The strip is an indication of sensible heat transfer from the duct wall to the solid PCM by pure conduction, taking the PCM from Solidus Temperature ($T_{sol} = 288.15 \text{ K}$ (15°C)) to Melting Point ($T_{mp} = 293.15 \text{ K}$ (20°C)). Subsequent heating of the PCM by the flowing air will take heat transfer within the PCM domain from conduction-controlled process to natural convection-controlled process. This progression of the heat transfer process within the PCM domain has a lot of impact on the cooling of the flowing air within the duct. The moment the heat transfer process changes from conduction-controlled to natural convection-controlled, heat transfer rate from the flowing air to the PCM was slowed down. Furthermore, molten PCM remains stagnant in the space between the duct wall and the yet-to-melt solid PCM, creating a sort of resistance to conductive heat transfer from the flowing air to the solid PCM.

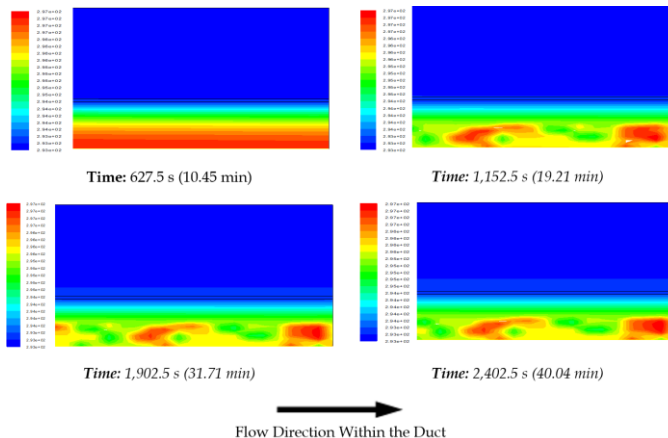


Figure 2: Contours of Static Temperature Near the duct outlet

The development of the liquid fraction of the PCM over time is shown as Contours of Liquid Fraction in Figure 3. About 10 minutes into the Air cooling process, the PCM domain is all deep blue ($\eta = 3.4\text{e-}01$) in colour as no observable melting has taken place. Conduction is the main heat transfer mechanism at this stage. As the melting progresses with time, the lighter blue ($\eta = 4.72\text{e-}01$) parallel strips of the melted region increase in thickness; another indication of a Conduction-controlled heat transfer process.

Further melting beyond 40 minutes will eventually take the melting to a natural convection-controlled process. The implication of the melting on the cooling process is that it slows down the heat transfer rate from air to the PCM. This is because liquid PCM has lower thermal conductivity than the solid PCM.

Figures 4a and b respectively confirm the hydrodynamic and thermal development of the air flow within the duct after 10 minutes of cooling; they show the varying cross-sectional profiles of the velocity and static temperature along the duct. These results are characteristic of developing laminar duct flow-assisted heat transfer, regardless of time.

Figures 4c and d respectively show the cross-sectional profiles of velocity and static temperature along the duct, but within the PCM container. The velocity profiles are characteristic of buoyant flow - very low values (between 0 and $2.5\text{E-}06$ m/s) and zig-zag pattern. The temperature profiles are typical of those for free convection heat transfer processes, with the highest value at the wall and the lowest high up in the container.

Figures 4e and f respectively show the mass weighted average velocity and static temperatures at axial locations within the air duct. Figure 4e indicates the kinetic energy state of air within the duct. This increases from inlet to outlet, while Figure 4f describes the thermal energy state of the air in the duct. This shows that the thermal energy reduces from the inlet to outlet of the duct.

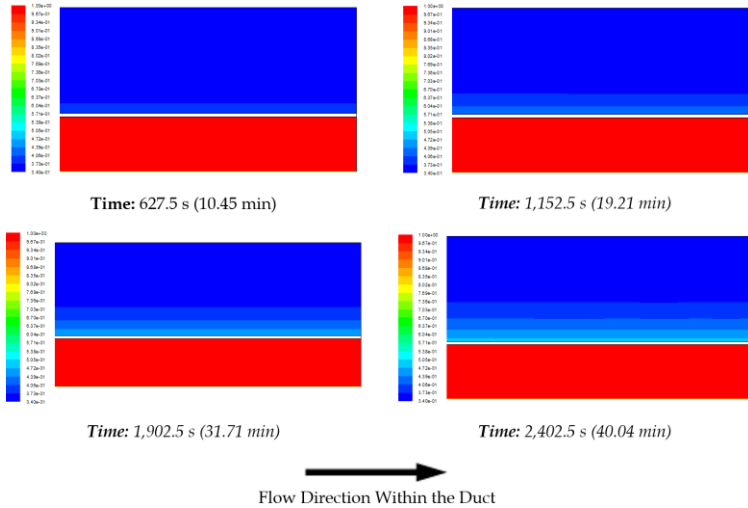


Figure 3: Contours of Liquid Fraction Near the duct outlet

Figures 4e and f respectively show the mass weighted average velocity and static temperatures at axial locations within the air duct. Figure 4e indicates the kinetic energy state of air within the duct. This increases from inlet to outlet, while Figure 4f describes the thermal energy state of the air in the duct. This shows that the thermal energy reduces from the inlet to outlet of the duct.

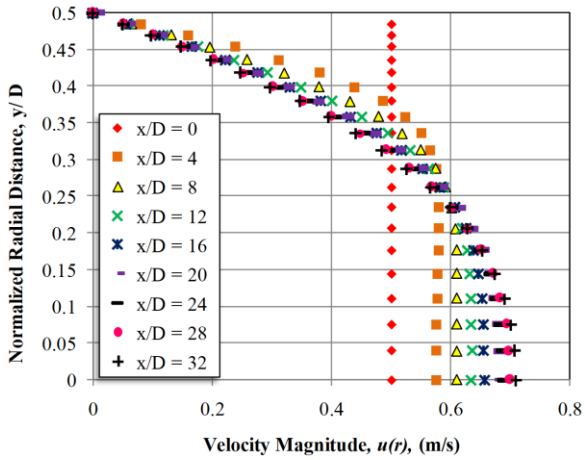


Figure 4a: Air Velocity Along the Duct length after 10 min of cooling

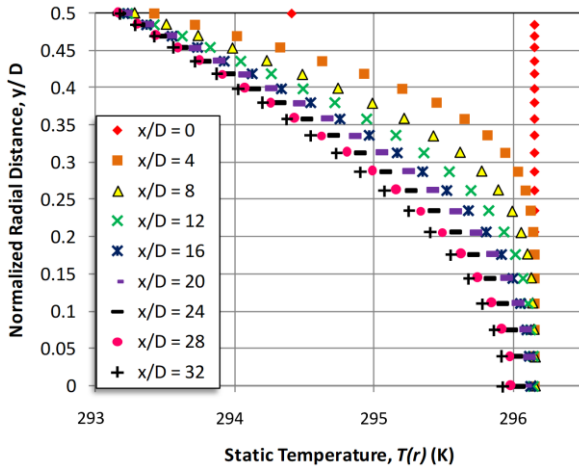


Figure 4b: Static Temperature Profiles at Axial locations Along the duct after 10 min of cooling

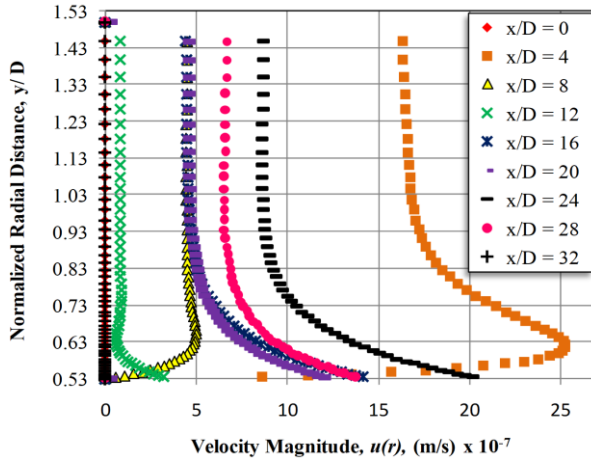


Figure 4c: Velocity Profiles at Axial locations Within PCM

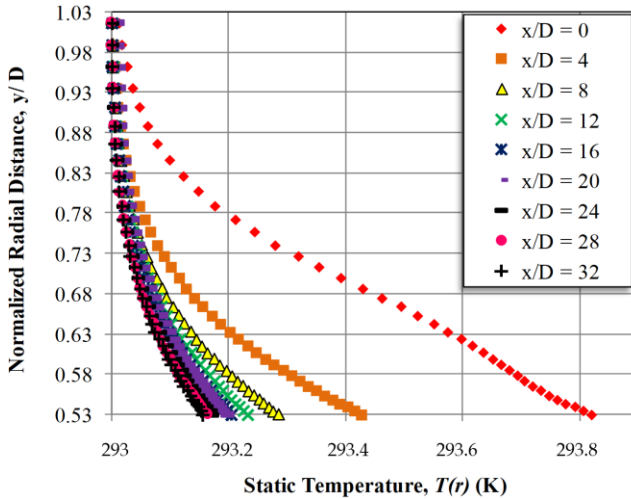


Figure 4d: Static Temperature Profiles at Axial locations Within PCM

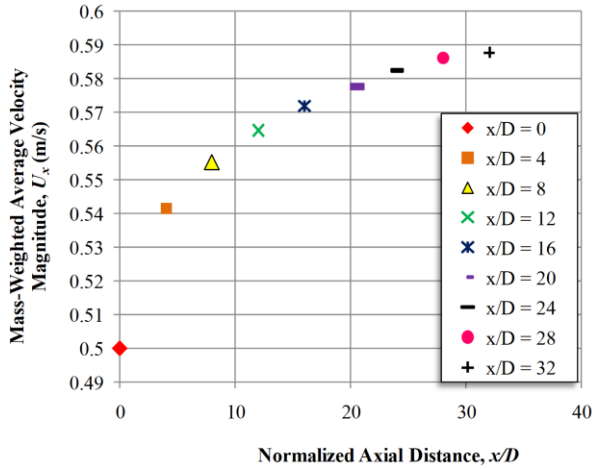


Figure 4e: Mass-Weighted Average Velocity Magnitude at Axial Locations Within the duct

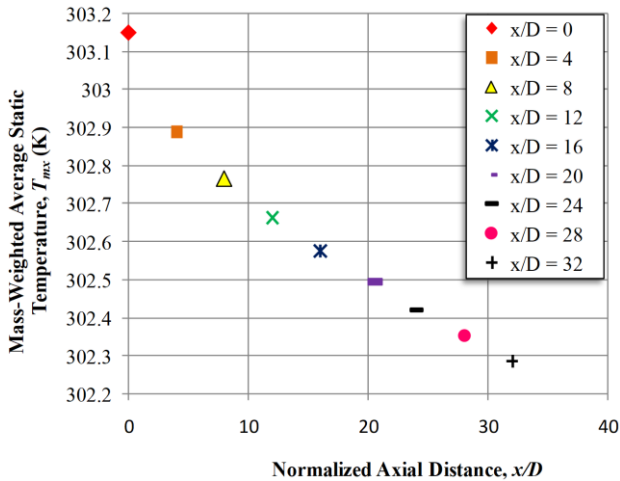


Figure 4f: Mass-Weighted Average Static Temperature at Axial Locations Within the duct

Equations (12) and (13) stated in section 2.2 were used to calculate Figures 4e and f respectively in (FLUENT manual, 2001), within the duct after 627.5 s (10.45 min.). Figure 4e shows the asymptotic growth of Mass-Weighted Average Velocity, U_x , towards fully developed value. This is the resultant effect of the growing hydrodynamic boundary layer, which reduces the flow cross-sectional area along x axis to conserve flow rate within the developing region. Figure 4f shows the linear reduction of Mass-Weighted Average Static Temperature, T_{mx} , towards fully developed value, axially. This is the resultant effect of the growing thermal boundary layer, which reduces the cross-sectional area available for thermal energy advection along x axis within the developing region. The ultimate goal of the energy transformation within the flow is to convert all the thermal energy available for advection at the duct inlet, to conductible thermal energy at fully developed region.

The effects of time on the static temperature profiles at the duct outlet ($x/D = 32$), within the PCM container is shown on Figure 5.

Temporal variations of liquid fraction within the PCM at the duct outlet cross section are shown in Figure 6. The shapes are similar to those for static temperatures presented in Figure 5. This is logical because Equation (8) in section 2.2 defines liquid fraction as a function of temperature.

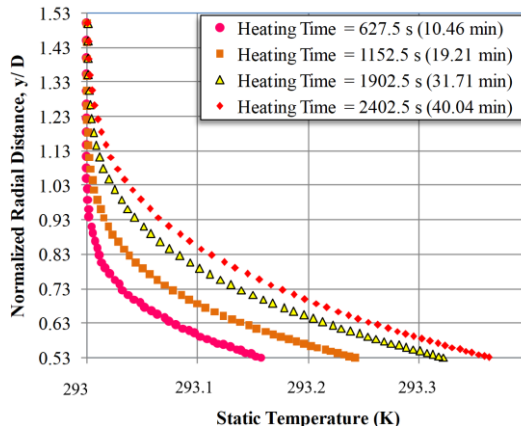


Figure 5: Temporal Static Temperature Profiles At $x/D = 32$ Within PCM

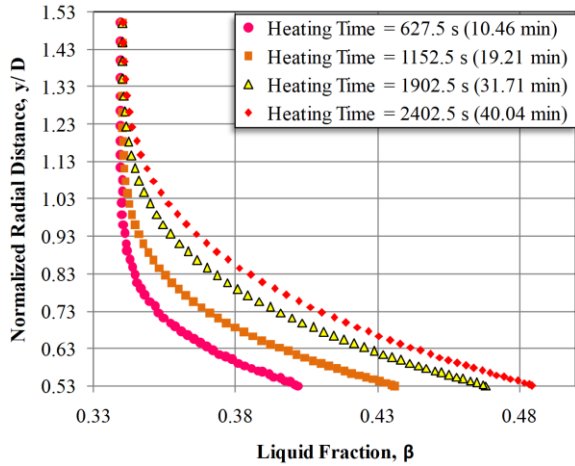


Figure 6: Temporal Liquid Fraction Profiles at $x/D = 32$ within PCM

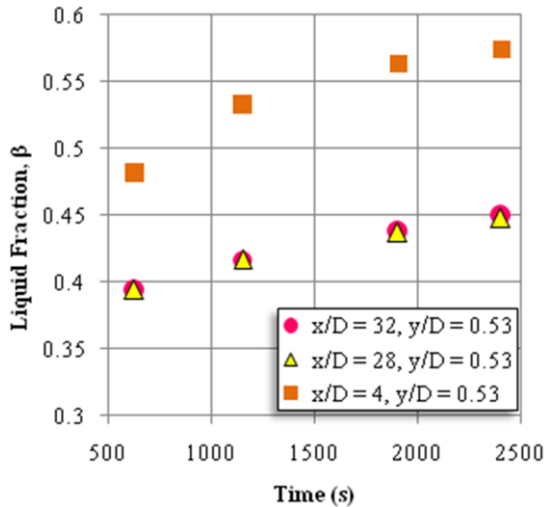


Figure 7: Temporal Wall Liquid Fraction Profiles Within PCM

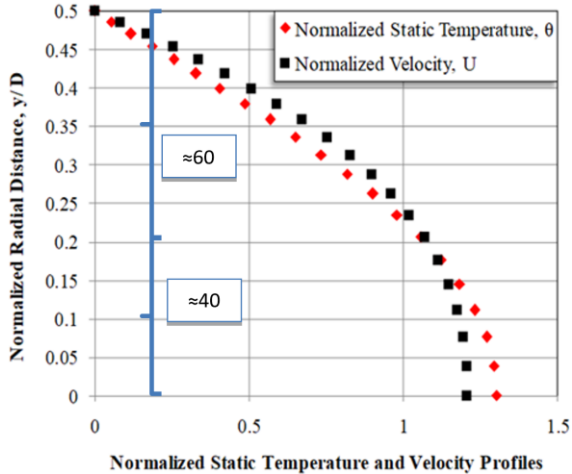


Figure. 8: Normalized Static Temperature and Velocity Profiles At $x/D = 32$ within Air Duct

Figure 7 is a derivative of Figure6; this shows the variation of liquid fraction and static temperature at the duct wall (PCM side), with time. It can be noticed that the rate of liquefaction / melting drops as the time increases; the highest rates on the curves are between 10 minutes (600sec.) and 19 minutes (1,140sec.), while the lowest rates (when the curve is being flattened) are between 31 minutes (1,860 sec.) and 40 minutes (2,400sec.). This confirms the fact that as the PCM melting process moves from conduction-controlled process to a free convection- controlled process, liquefaction rate of the PCM is reduced, then the transfer rate between the Air and OPCM is subsequently reduced; and thus the cooling rate of the flowing air decreases

Figure 8 shows the normalized profiles of Static Temperature, $\theta = \frac{T_w - T(r)}{T_w - T_{mo}}$, and Velocity $U = \frac{u(r)}{U_x}$, at the outlet of the air duct. This shows that the thermal boundary layer (in red) is thicker than the velocity boundary layer (in black). And since Prandtl Number is:

$$\frac{V}{\alpha} = \frac{\text{Viscous}_{-}\text{diffusion}_{-}\text{rate}}{\text{Thermal}_{-}\text{diffusion}_{-}\text{rate}} < 1$$

Hence this confirms the fact that Prandtl number, $Pr=0.7 < 1$ for air (Kay W. et al. 2005; Dolado P et al. 2011). The controlling parameter is however the velocity, because it has higher gradient at the wall.

4.0 Conclusion

Transient numerical simulations were performed to investigate the heat transfer process between ambient space air and a colder bio-based Organic Phase Change Material (*PureTemp20*) in an OPCM-Air heat exchanger configuration. The air flows from the return air of an Air-conditioned space at a Reynolds number of 1,569 and temperature of 297.15K (24°C) into a circular duct embedded in the OPCM material, and all are enclosed in a rectangular container. The following can therefore be deduced from the numerical investigation:

- i. The numerical simulations of Instantaneous air flow velocity $u(r)$ distributions and Instantaneous Static Temperature $T(r)$ profiles (Figures 4a and 4b in section 3.0) were found to be in agreement with the shapes in (Kay et al., 2005) within the hydro-dynamically and thermally developing region.
- ii. The qualitative result shown in Figure 2 and the quantitative result in Figure 7 above indicate that the heat transfer from Air to OPCM starts at the OPCM's solidus temperature with conduction-controlled heat transfer process (CDC-HTP), and as the OPCM starts to melt, Free Convection-controlled heat transfer process (FCC-HTP) set in, while the effect of CDC-HTP is minimal. With time (about 40mins) the effect of the FCC-HTP is pronounced and the liquefaction rate of the OPCM is drastically reduced, and thus the heat transfer from the air flow to OPCM also decreases.
- iii. **Figure 8** shows that the thermal boundary layer is thicker than the velocity boundary layer in the air duct. Thus, Prandtl number (Pr) of air is less than 1. This confirms Prandtl number $Pr=0.7 < 1$ (Kay et al., 2005; Dolado et al., 2011).

5.0 Recommendations

The following are the suggested recommendations on this research work. First, since Conduction-Controlled heat transfer process is the major means by which heat is effectively transferred between the flowing Air and the OPCM in the heat exchanger under consideration, the circular duct should be externally finned to enhance the heat transfer process. Secondly, the qualitative and quantitative results obtained during this numerical investigation are useful data for further research references.

6.0 Nomenclature

Alphanumeric Symbol	Description	Alphanumeric Symbol	Description
A	Duct Cross Sectional Area (m^2)	$U_x(x)$	Mass-Weighted Average velocity at axial locations
A_c	Porosity Function (kg/m^3s)	$v(r)$	Instantaneous flow velocity - radial component of fluid
B	Computational Constant (-)	\vec{V}	Fluid Velocity (m/s)
C	Mushy Zone Constant (kg/m^3s)	x	Axial Co-ordinate (m)
C_p	Specific Heat at constant pressure (J/kgK)	$x_{d,h}$	Hydrodynamic Entry Length
$^{\circ}C$	Degree Celsius	$x_{d,t,h}$	Thermal Entry Length
D	Duct Wall Thickness (m)		
D	Duct Internal Diameter (m)	Greek letters	Description
2-D	Two-dimensional	μ	Absolute Viscosity ($kg/m\cdot s$)
H	Total Enthalpy (J/kg)	ρ	Density (kg/m^3)
H_s	Sensible Enthalpy (J/kg)	ν	Kinematic Viscosity, $\nu=\mu/\rho$
H_{lat}	Latent Enthalpy for the phase change in a numerical control volume ($l/L\omega$)	β	Liquid Fraction
HVAC	Heating, Ventilating and Air-Conditioning	α	Thermal Diffusivity, $\alpha =k/\rho C_p$
K	Thermal Conductivity (W/mK)	Subscripts	Description
K	Kelvin	E	Energy balance
L	Latent Heat of fusion (J/kg)	fd,h	Hydrodynamically fully
P	Static Pressure (N/m^2)	fd,th	Thermally fully developed
PCM	Phase Change Material	i	Inlet
Pr	Prandtl Number, $Pr = \mu C_p/k$	lat	Latent
Q	Volume flow rate, $Q = AU_i(m^3/s)$	liq	Liquidus
R	Radial Co-ordinate (m)	mx	Mass-Weighted Average value
Re_D	Reynolds Number, $Re_D = U_i D/\nu$	mo	Mass-Weighted Average value
S_M	Source Term momentum equation (N/m^3)	M	Momentum balance
S_E	Source Term energy equation (J/m^3s)		

Alphanumeric Symbol	Description	Subscripts	Description
T	Time (s)	<i>ref</i>	Reference
$T(x,r)$	Instantaneous Static Temperature (K)	<i>s</i>	Sensible
T_i	Free Stream Static Temperature at duct inlet	<i>sol</i>	Solidus
T_{liq}	Liquidus Temperature (K)	<i>CDC-HTP</i>	Conduction-controlled Heat fer Process
$T_{ms}(x)$	Mass-Weighted Average Static Temperature at axial locations (K)		
T_{mo}	Mass-Weighted Average Static Temperature at duct outlet (K)	<i>FCC-HTP</i>	Free Convection-controlled Heat Transfer Process
T_{mp}	Melting point of PCM (K)		
T_{sol}	Solidus Temperature (K)		
$u(x,r)$	Instantaneous flow velocity - axial component of fluid velocity (m/s)		

7.0 References

- Abduljalil A. A., Sohif B.M., Sopian K., Sulaiman M.Y., Abdulrahman TM. , 2013, "CFD applications for latent heat thermal energy storage: a review" *Renewable and Sustainable Energy Reviews* **20**, 353-363.
- Adel W., Zia D., 2013, "Phase change material (PCM) storage for free cooling of buildings – A review" *Renewable and Sustainable Energy Reviews* **18** 607-625.
- Chen D., Zhiling N., Bingwei L., Dongpao H., Zijun Z. and Muchun Y., 2020, "Analytical modeling and thermal performance analysis of a flat plate latent heat storage unit" *Appl. Therm. Eng.* **179** 115722.
- Dolado P, Lazaro A., Marin J. M. and Zalba B., 2011, "Characterization of melting and solidification in a real scale PCM-air heat exchanger: Numerical model and experimental validation" *Energy Convers. Manag.* **52** 1890-1907.
- Dubovsky V., Ziskind G. and Letan R., 2011, "Numerical Study of a PCM-Air Heat Exchanger's Thermal Performance" *Appl. Therm. Eng.* **31** 3453-62.
- Ezra M, Kozak Y., Dubovsky V. and Ziskind G., 2016, "Analysis and optimization of melting temperature span for a multiple-PCM latent heat thermal energy storage unit" *Appl. Therm. Eng.* **93** 315-329.
- Fallahnezhad N. and Nasif HR., 2020, "Numerical Solution of Transient Freezing Equations of a Laminar Water Flow in a Channel with Constant

Wall Temperature in the Absence of Gravity" *Microgravity Science and Technology***32**, 493–505.

FLUENT Manual, Chapter 21: Modeling Solidification and Melting; ANSYS, Inc.: Canonsburg, PA, USA, 2001.

Gowreesunker B L., Tassou S. A. and Kolokotroni M., 2013, "Coupled TRNSYS-CFD simulations evaluating the performance of PCM plate heat exchangers in an airport terminal building displacement conditioning system" *Build. Environ.***65** 132-145.

Guo L., Hang S., Uwe K., Hannah M., Markus A., Min S., Ulrich P. and Yafang C., 2018, "Technical note: Influence of surface roughness and local turbulence on coated-wall flow tube experiments for gas uptake and kinetic studies", *Atmos. Chem. Phys.*, **18**, 2669–2686.

Hameter, M.; Walter, H., 2016, "Influence of the mushy parameter on the numerical simulation of the melting and solidification process of phase change materials". *In Proceedings of the 26th European Symposium on Computer Aided Process Engineering, Portorož, Slovenia.*

Herbinger, F. et al., 2016, "Numerical study of a PCM-air heat exchanger's thermal performance," *Journal of Physics, Conference Series.* **745** 032127.

Herbinger, F., Bhourri, M. & Groulx, D., 2018, "Investigation of heat transfer inside a PCM-air heat exchanger: a numerical parametric study". *Heat and Mass Transfer***54** 2433–2442.

Kays, W. M., 2011, "Convective Heat and Mass Transfer" Mcgraw-Hill Education (India) Private Ltd.

Kays, W. M., Crawford, M. E. and Weigand, B., 2005, "Convective Heat and Mass Transfer" Mcgraw-Hill Series in Mechanical Engineering Education, Boston 4th ed.

Koller M., Walter H., Hameter, M.; 2016 "Transient Numerical Simulation of the Melting and Solidification Behavior of NaNO₃ Using a Wire Matrix for Enhancing the Heat Transfer". *Energies***9**, 205.

Labat M., Virgone J., David D. and Kuznik F., 2014, "Investigation of heat

transfer inside a PCM-air heat exchanger: a numerical parametric study". *Appl. Therm. Eng.* **66** 375-382.

Langhaar, H. L., 1942, "Laminar Flow in the Entrance Region of a Smooth Pipe" *Journal of Applied Mechanics*, **64**, A-55.

Pure Temp 20 Technical Data Sheet; Entropy Solutions, LLC. 4232 Park Glen Road, Minneapolis, MN 55416.

Vakalaltojjar S. M. and Saman W., 2001, "Analysis and Modeling of Phase Change Storage System for air Conditioning Applications" *Appl. Therm. Eng.* **21** 249-263.

Voller, V.R.; Prakash, A., 1987, "A fixed grid numerical modelling methodology for convection-diffusion mushy region phase-change problems". *Int. J. Heat Mass Transf.*, **30**, 1709-1719.

Zalba B, Marin J. M, Cabeza L. F. and Mehling H., 2004, "Free Cooling of Buildings with Phase Change Materials" *Int. J. Refrig.* **27** 839-849.